ADVANCED FUNCTIONAL MATERIALS
www.afm-journal.de

Wide-Area Strain Sensors based upon Graphene-Polymer Composite Coatings Probed by Raman Spectroscopy

Arun Prakash Aranga Raju, Amanda Lewis, Brian Derby, Robert J. Young, Ian A. Kinloch, Recep Zan, and Kostya S. Novoselov*

Functional graphene optical sensors are now viable due to the recent developments in hand-held Raman spectroscopy and the chemical vapor deposition (CVD) of graphene films. Herein, the strain in graphene/poly (methyl methacrylate) sensor coatings is followed using Raman band shifts. The performance of an "ideal" mechanically-exfoliated single crystal graphene flake is compared to a scalable CVD graphene film. The dry-transferred mechanically exfoliated sample has no residual stresses, whereas the CVD sample is in compression following the solvent evaporation during its transfer. The behavior of the sensors under cyclic deformation shows an initial breakdown of the graphene-polymer interface with the interface then stabilizing after several cycles. The Raman 2D band shift rates per unit strain of the exfoliated graphene are ≈35% higher than CVD graphene making the former more strain sensitive. However, for practical wide-area applications, CVD graphene coatings are still viable candidates as a Raman system can be used to read the strain in any 5 μm diameter spot in the coating to an absolute accuracy of ≈0.01% strain and resolution of ≈27 microstrains (μs), which compares favorably to commercial photoelastic systems.

1. Introduction

The monolayered nature of graphene makes it of particular promise for sensor applications as every atom is present at both surfaces, increasing its sensitivity to environmental changes. For example, the Hall effect has been used in gas sensing to detect the absorption of single NO_2 and NH_3 molecules.[1] Graphene has also been used as a photo detector.[2,3] Micro-engineered vibrating beam sensors have taken advantage of graphene's high stiffness and low density to act as mass sensors with detection limits up to 2 zeptograms.[4] Graphene has also shown promise as a peizo-restivity based strain sensor, with studies based on mechanically exfoliated,[5,6] chemical vapor deposition (CVD)-grown[7–11] and composites.[12,13] CVD graphene on polydimethylsiloxane (PDMS) had a gauge factor (GF) of 6.1[7] whilst exfoliated graphene on PDMS had a GF ≈ 2 for applied strains up to 30%.[6] In a very recent study, thin films, produced by spray coating of liquid-phase exfoliated graphene, on a plastic substrate were used to demonstrate strain sensitive coating with a tunable gauge factor based on the stretching of a percolated graphene network.[14] These sensors are analogous to the conventional foil strain gauges (GF 2–5) which give high accuracy single-point measurements.[15]

In addition to high accuracy, single-point, deformation measurements, there is a need to be able to measure local strain at multiple points over a structure. Whilst this can be achieved with electronically-based sensors, every point of interest needs to be individually wired, leading to a significant amount of infrastructure. Thus it is preferable to measure the strain using optical measurements based upon the photoelastic properties of either the material itself or an active coating upon it. A classic example of such a system is the birefringence measurements made on poly (methyl methacrylate) (PMMA) and polystyrene (PS) structures. There are already commercially available photoelasticity-based sensors, such as the Grey-field Polariscope from Stress Photonics and PhotoStress from Vishay Precision Group.[16] In these techniques, photoelastic sensitive coatings based on PS/epoxy resin are applied over complex structures and a polariscope measures the strain-induced birefringence to form a full-field strain map with resolutions from 10 to 20 microstrains ($\mu\varepsilon$) (see manufacturer's data sheet).[16] Bragg diffraction gratings are another option but require a complex fiber optical lay-up to achieve sufficient point resolution over a large area.[17] A promising rival to these optical systems is the development of Raman active coatings, where a strain active material is coated onto a device and the strain is read using a hand-held Raman spectrometer. This technique relies on the sensitivity of the Raman bands to the bond strain; tension causes frequency downshift (phonon softening) while the compression causes frequency upshift (phonon hardening).

The development of the Raman strain sensors has been limited due to the lack of hand-held spectrometers and the

A. P. A. Raju, A. Lewis, Prof. B. Derby, Prof. R. J. Young, Prof. I. A. Kinloch, Dr. R. Zan
School of Materials
University of Manchester
Grosvenor Street, Manchester, M13 9PL, UK
E-mail: ian.kinloch@manchester.ac.uk
Prof. K. S. Novoselov
School of Physics and Astronomy
University of Manchester
Oxford Road, Manchester, M13 9PL, UK

DOI: 10.1002/adfm.201302869

development of suitable active coatings. Raman systems, however, are now available based upon solid-state lasers for under $15k. Earlier studies on Raman active coatings focused upon using carbon nanotubes. Wagner et al. used single-walled carbon nanotubes (SWNT) as Raman sensors in glass fiber polymer composites to measure the stress concentrations around defects and demonstrated that the nanotubes could be used to produce a two-dimensional mapping of the strain distribution in the composite.[18,19] Sureeyatanapas et al. demonstrated that SWNTs could be incorporated into the sizing of glass fibers to give a strain sensitive coating.[19] It was found that functionalized SWNT showed higher strain sensitivity due to a better interface with the sizing. Li et al. demonstrated the use of nanotube as macro-scale strain sensors in Bucky papers by both Raman and electrical measurements.[20] Following this work, Vega et al. developed SWNT-epoxy coatings as strain sensors by simultaneously following Raman spectroscopic and electrical impedance measurements.[21] The impedance and Raman response of these coatings followed each other in single-cycle deformation experiments. Whereas, when subjected to cyclic deformation, the Raman method gave information about the interfacial damage.[21]

It has been suggested by ourselves[22,23] and others,[24,25] that graphene would be the ideal Raman active coating and superior to CNTs due to 1) graphene's two-dimensional nature making it more suitable for coatings, 2) the higher inherent band shift per unit strain of the 2D Raman band in graphene,[26] 3) the high intensity of graphene's most strain sensitive band (2D band). Recently Reserbat-Plantey et al. showed that graphene's suitability for sensing was such that even real time dynamic measurements could be taken from a single point.[27] However, to date graphene has not been studied as a wide area strain sensor, partly due to a lack of suitable material; mechanically-exfoliated graphene as demonstrated herein works well but is not scalable, whereas, solvent-exfoliated graphene is shorter than the critical length of graphene required for efficient stress transfer meaning that no strain is transferred from the composite to the flake (this critical length effect is demonstrated in Supporting Information).[22] In the last few years, though, large area CVD films have become available and Sony Corporation has demonstrated roll-to-roll production and transfer of a 100 m long graphene films.[28] In the present novel study, we use a mechanical exfoliated flake as a model single grain system and then compare its performance to CVD graphene on a polymer backing, which is being readily scaled in manufacture by a number of companies and groups.[28–30] The shift of the Raman 2D band with strain under cyclic deformation was followed to determine the in-service behavior of the sensor coating. In particular, the interfacial characteristics of the graphene-polymer interface were studied during the cyclic deformation as these determine the stress transfer to the graphene and hence its strain sensing ability. These measurements also have significance for the wider graphene composite community, particular on the fatigue behavior of such materials. Finally, we calculate the absolute accuracy and resolution of the graphene-based Raman strain sensor as a function of graphene source.

2. Results and Discussion

2.1. Coating Characterization

Composite coatings were prepared from both mechanically exfoliated (herein termed "exfoliated") and CVD-grown graphene. **Figure 1**a show the schematics of the sample preparation (see Experimental Section). The in situ Raman measurements were carried out on the graphene monolayer flakes as shown in the optical micrographs (see Supporting Information Figure S1). Well-defined Raman spectra with a characteristic 2D band (around 2640 cm^{-1}), G band (around 1580 cm^{-1}), and D band (1350 cm^{-1}) were obtained from both the exfoliated and CVD graphene. Figure 1b show the example flakes found in the composite system with increasing number of layers, with the $I_{2D/G}$ ratio greater than 3 for the monolayer graphene. The absence of a D band for the exfoliated graphene reveals its high-quality.[31] Figure 1c shows the Raman spectra of as-grown CVD graphene on Cu foil and in the coatings. $I_{2D/G}$ ratio was greater than 2 and the full-width-of-half-maximum (FWHM) of ≈25 cm^{-1}.

Scanning electron microscopy was used to measure the grain size in the CVD graphene. The residual impressions of the copper grain boundaries were clearly visible in the transferred film at very low magnifications. However, close inspection within these residual copper grain impressions found that the actual grain size of the graphene was 7.3 ± 4.8 μm (see Supporting Information Figure S2). Wrinkles and damage were also observed in the film as a result from the transfer process.

2.2. Cyclic Deformational Behavior

2.2.1. Sequence I: Uniform Maximum Strain Levels

The coatings were subjected to cyclic deformation using a four-point bending rig with the maximum strain of 0.3% at each cycle. **Figure 2**a,d show the deformation sequence applied and the response of the 2D band position. The Raman 2D band shifts significantly with the applied strain, indicating that stress transfer occurred in the coatings (Figure 2b,e). Elastic deformation occurred in the exfoliated graphene coatings, with the loading and unloading curves for the first cycle overlaying each other. The shift rate of –53 cm^{-1}/% strain (Figure 2c) was obtained for both loading and unloading curve is similar to the previous studies.[24,26] As the sample undergoes subsequent deformation cycles, the linearity between the loading and unloading curve is lost, giving rise to a hysteresis loop. This behavior can be related to the coatings undergoing damage at the graphene-matrix interface. Cyclic deformation of bulk carbon nanotube composites revealed similar behavior due to damage at nanotube-matrix interface.[32] The hysteresis loop increases in area and shifts upwards with the deformation cycle (see Supporting Information Figure S4). This behavior suggests that the coating underwent irreversible damage at the graphene-matrix interface. Furthermore at the end of each cycle, the 2D band position at 0% strain is at higher wavenumber than in the previous cycle. This is consistent with graphene undergoing slippage during the loading cycle and then in-plane

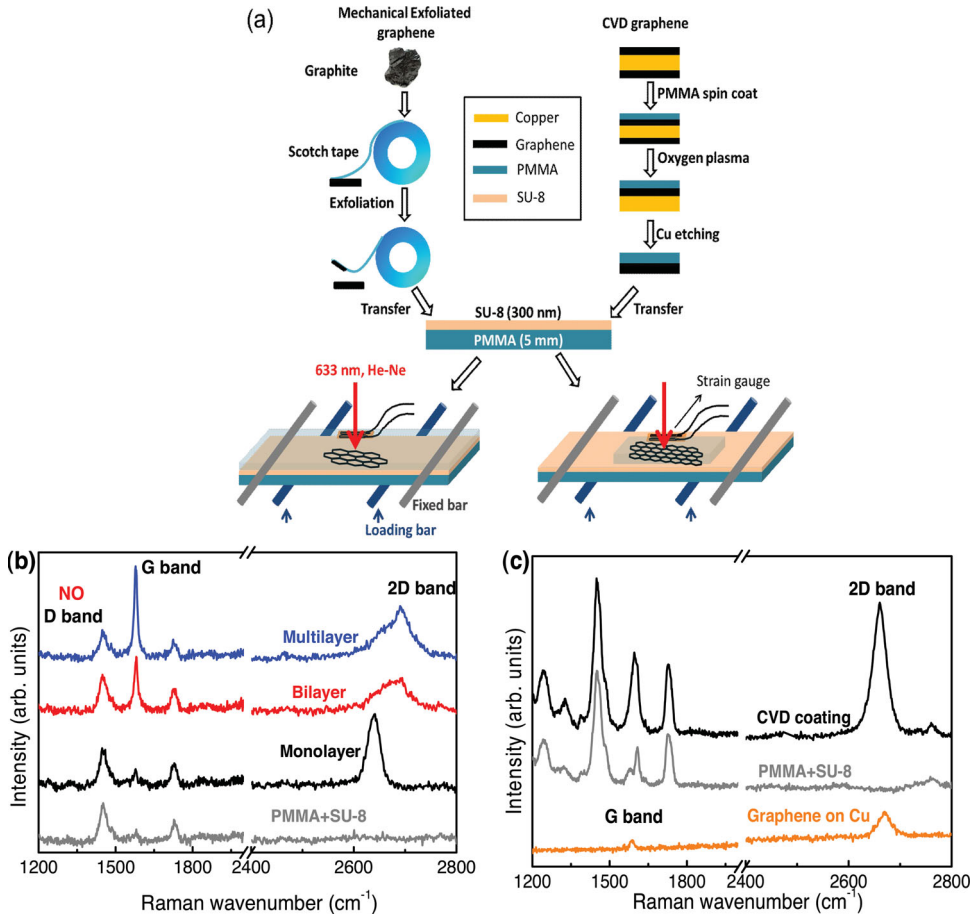

Figure 1. a) The schematic representation of the model composite coatings preparation. b) Raman spectra of different layers of graphene in exfoliated composite coatings. The shape of 2D band varies with the number of graphene layers; monolayer could be fitted with a single Lorentzian, whereas the band splits into four for bilayer.[31] Absence of D band at ≈1350 cm^{-1} indicates high crystalline order of the sample. c) Raman spectra of the as-produced CVD graphene on Cu foil and in the composite coating. The spectra from PMMA top coat and SU-8 is shown as a reference in both cases. Spectra offset for clarity.

compression during unloading, resulting in the development of residual compression.

The initial 2D band position was significantly higher in the CVD coating (≈2660 cm^{-1}) compared to exfoliated graphene (≈2640 cm^{-1}), indicating that the CVD graphene was under residual pre-compression. This residual pre-compression was found throughout the sample, with the average band position being ≈2659.7 ± 2.5 cm^{-1} over 200 random spots. The residual pre-strain is believed to be developed from the transfer process and drying of the PMMA top coat.[33] The initial two deformation cycles had allowed the graphene to relax this pre-compression (Figure 2d,e). From the third cycle onwards, approximately elastic deformation occurs, indicating good stress transfer between the graphene and matrix. Unlike in the exfoliated graphene, the 2D band position at 0% strain is constant at the end of the final three deformation cycles, indicating no further significant relaxation of residual strains.

The theoretical ideal shift rates for graphene is calculated by using the Gruneisen parameter, γ, which is a measure of rate of change of phonon frequency in a crystal with strain.[33] For the uniaxial strain the Gruneisen parameter of 2D band (γ_{2D}) could be defined as,

$$\gamma_{2D} = -\frac{1}{\omega^0_{2D}} \frac{\Delta\omega_{2D}}{\varepsilon(1-\upsilon)} \quad (1)$$

where, $\Delta\omega_{2D}/\varepsilon$ is the shift rate of 2D band, $\omega^0{}_{2D}$ is initial position of 2D band before straining and υ is the Poisson's ratio. In the literature, various values of Gruneisen parameters are reported and it is still a matter of argument.[35,36] The Poisson's ratio of the polymer coatings was used 0.33 as the graphene exhibited elastic deformation indicating good adhesion between graphene and the substrates once the residual strain had been annealed. This ratio was taken as 0.33 as the Poisson ratio of PMMA is 0.3–0.35 and SU-8 is a transversely isotropic material with an in-plane Poisson ratio of 0.33. We took the Gruneisen parameter value as 2.7 as calculated by the first-principle calculations of Mohiuddin et al.[34] Ideal shift rates of –62 cm^{-1}/% strain (Figure 2c,f) were obtained for both exfoliated and CVD graphene which is similar to the value (≈–60 cm^{-1}/% strain) reported in the published literature.[24,26,34,37]

The shift rates of both loading and unloading curves of exfoliated graphene increases with the deformation cycles and reached the theoretical ideal shift rate (Figure 2c). This behavior could be related to the strain hardening of the graphene,

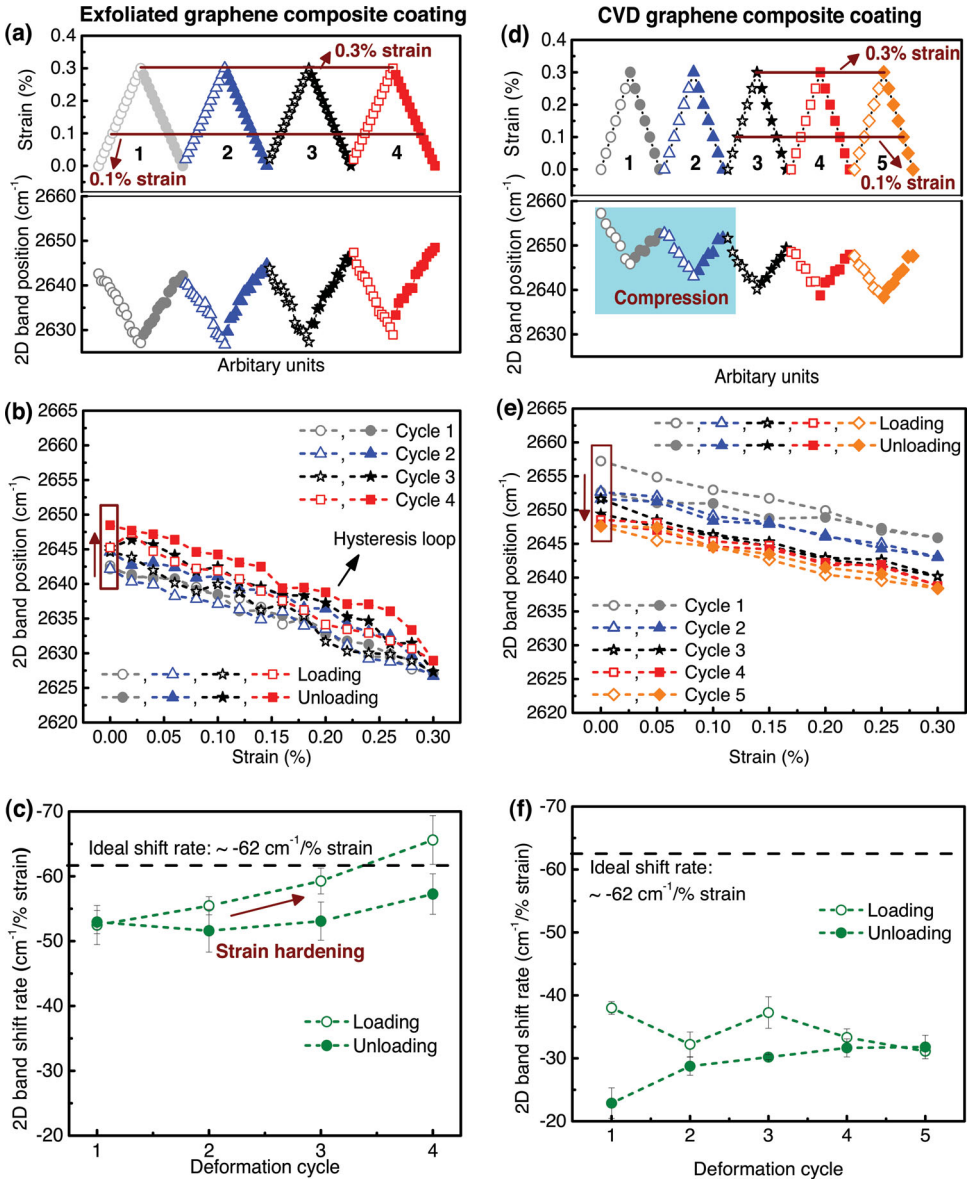

Figure 2. Sequence I cyclic deformation with uniform maximum strain level. a,d) The sequence of the deformation and the response of 2D band position of both exfoliated and CVD graphene. The highlighted area shows the relaxation of residual pre-compression of CVD graphene in the initial two cycles. The strain sensing ability was calculated at 0.1% and 0.3% strain levels as indicated. b,e) The shift of 2D band vs loading strain. The hysteresis loop observed in the exfoliated graphene indicates the interfacial damage. Boxes at 0% strain indicate the behavior of the residual stresses at the end of the deformation cycles. c,f) Shift rate of 2D band, obtained from slopes of (b,e). The dashed horizontal line indicates the theoretical ideal shift rate calculated by using the Gruneisen parameter ($\gamma = 2.7$).

meaning graphene exhibits more resistance to the deformation in the subsequent deformation cycles. The reason for this behavior is unclear at this point, but the flattening of the ripples present in the graphene during the deformation could be one plausible explanation. Whereas for the CVD graphene, the shift rate is approximately half of the theoretical ideal shift rate ≈–30 cm^{-1}/% strain. This shift rate, however is lower than the results of –72 cm^{-1}/% strain from stretching CVD graphene on PDMS. It should be noted that the work of Bissett et al. using a more deformable substrate (PDMS) leading to biaxial deformation and thus is not directly comparable.[38] Furthermore since Bissett et al. were not able to accurately measure the strain in their PDMS substrate, they assumed that their exfoliated and CVD graphene would have the same band shift rate.[38]

The Raman band shift could be used to estimate the effective Young's modulus of the graphitic based carbon reinforcements. As mentioned before, for uniaxial strain, the common shift rate obtained/calculated is ≈–60 cm^{-1}/% for 1 TPa monolayer graphene.[24,26,34,37] From the shift rates obtained in Figure 2c,f, the average effective modulus of exfoliated graphene and CVD graphene are in the order of ≈0.93 ± 0.1 TPa and ≈0.52 ± 0.12 TPa, respectively.

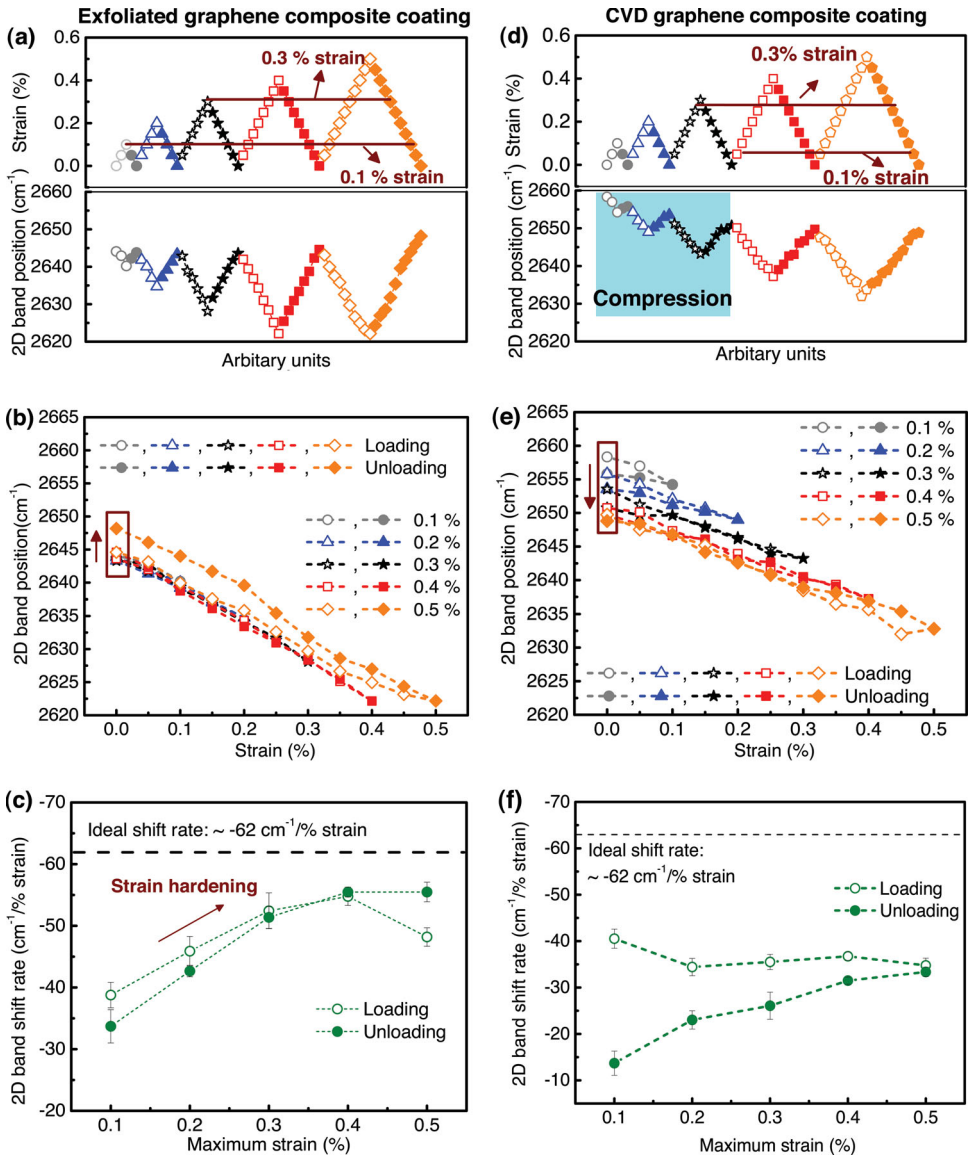

Figure 3. Sequence II cyclic deformation with increased maximum strain level a,d) The sequence of the deformation and the response of 2D band position of both exfoliated and CVD graphene. The highlighted area shows the relaxation of residual pre-compression of CVD graphene in the initial three cycles. The strain sensing ability was calculated at 0.1% and 0.3% strain levels as indicated. b,e) The shift of 2D band vs loading strain. Boxes at 0% strain indicate the behavior of the residual stresses at the end of the deformation cycles. c,f) Shift rate of 2D band, obtained from slopes of (b,e). The dashed horizontal line indicates the ideal shift rates calculated by using the Gruneisen parameters ($\gamma = 2.7$).

2.2.2. Sequence II: Increased Maximum Strain Levels

In this section, the coatings were subjected to deformation with increased maximum strain levels. **Figure 3**a,d show the deformation sequence used and the response of the 2D band position of both exfoliated and CVD graphene coatings. The significant shift of 2D band with applied strain as seen in Figure 3b,e indicates that the stress transfer occurred in the coatings. For the exfoliated graphene, the 2D band shifts approximately linearly with the strain up to 0.4% strain. When the strain level increased to 0.5%, the loading and the unloading curve do not superimpose indicating the onset of the interfacial damage in the coating and leading to the hysteresis loop. Also, similar to the previous deformation sequence, the 2D position at the 0% strain level at the end of the deformation cycle is at a higher wavenumber than the previous cycle (see Figure 3b). This indicates that the graphene is undergoing slippage during the loading cycle leading to the development of residual compression at the end of the cycle. The shift rates calculated from the slope of Figure 3b is plotted in Figure 3c. Strain hardening was observed with each cycle, as seen in the previous deformation sequence.

As before, the as-made CVD graphene coating had residual compression, leading to a relatively high 2D band position (≈2660 cm^{-1}). The initial deformation cycles (see Figure 3d,e) allowed the graphene to relax the pre-strain, after which the

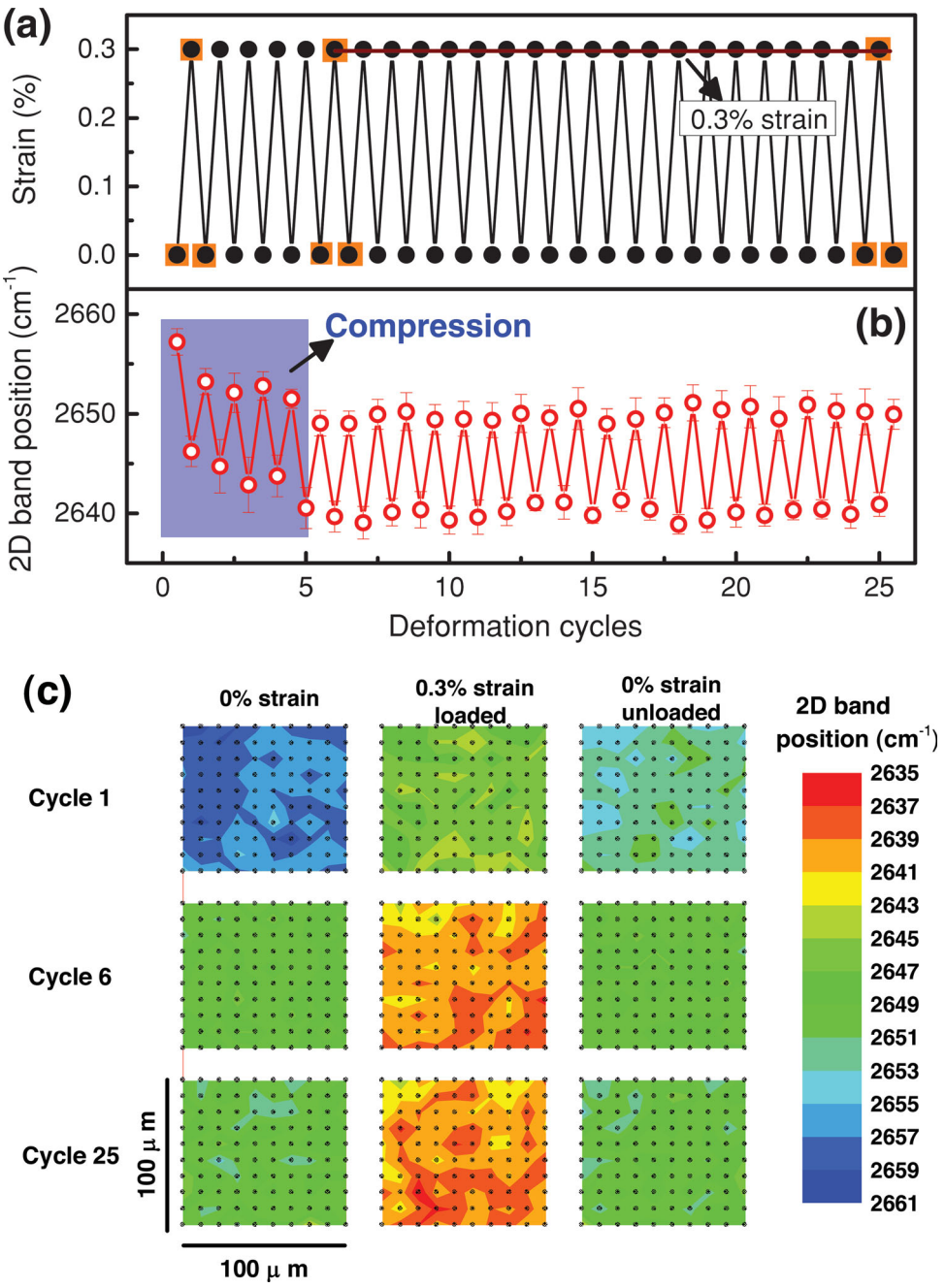

Figure 4. a) The deformation cycle applied to a CVD composite coating over 25 cycles. The highlighted points are the points in the cycle where a full Raman map was taken in (c). The strain sensing ability was calculated at 0.3% strain as indicated. b) The average Raman position in the 100 μm × 100 μm region of interest, based on five spectra taken from random locations. c) Raman maps of the 2D band position. The black spots represent the place where the spectra were obtained (error ± 2 μm).

coating exhibited almost elastic deformation. The 0% 2D band position of last three deformation cycles remains almost constant around ≈2650 cm^{-1} suggesting no further relaxation of residual strain. The average shift rate per unit strain was –31 ± 7.9 cm^{-1}/% strain, which is ≈35% lower than the exfoliated graphene (–48 ± 7.5 cm^{-1}/% strain) . The reason for the lower shift rate might be the many fine grain structure of the CVD graphene.

2.2.3. Sequence III: Mapping of Strain Over a Wide Area of CVD Graphene

In order to demonstrate both the spatial strain mapping ability and life time of the graphene sensors, a CVD graphene coatings was deformed for 25 cycles using the sequence shown in **Figure 4**a. The average 2D position within the 100 square

micron region of interest is shown in Figure 4b. As seen in previous samples, the film was initially in compression, with this compression being relaxed over the first few cycles of deformation. The strain response of the film was then found to be stable for the rest of the experiment with the maximum and minimum peak positions were constant within error. The 2D band position was also manually mapped at the start (0% strain), mid-point (0.3% strain), and end (0% strain) of the initial, 6th, and 25th cycles (Figure 4c). The mapping was taken at step intervals of 10 ± 2 μm and confirm that the residual pre-compression relaxes over the first few deformation cycles to give a stable system. In particular, the Raman maps for cycles 6 and 25 are very similar confirming that the strain behavior of the graphene film stabilizes. As noted earlier, the grain size of graphene film is approximately 7 μm, hence the mapped region corresponds to approximately 14 randomly orientated grains in each direction. Therefore the relative uniformity of the Raman band position strongly suggests that individual grain orientation relative to the direction of deformation is not a significant factor in the strain response.

2.3. Discussion: Comparison of Micromechanics of Exfoliated and CVD Graphene

In the current study, exfoliated and CVD graphene coatings were subjected to various cyclic deformation sequences to understand their deformation behavior. It can be seen from the results that, the residual pre-strains (mainly from the transfer process) present in the graphene flakes play a major role in their mechanical behavior as identified previously by other research groups.[24,25,33,34,39,40] For example, Fu et al. reported a slight decrease in the electrical resistance in initial stretching cycles followed by an increase in resistance in the subsequent cycles which they attributed to the relaxation of residual strains in the transferred CVD/PDMS film.[8] In general, in all the experiments residual pre-compression was observed in CVD graphene which relaxes over the initial few deformation cycles. Whereas, the exfoliated flake initially had relatively little pre-strain.

However, in general, the shift rates of exfoliated graphene were at least ≈35% higher than the CVD graphene. In order to understand this difference, the structure of the two materials needs to be considered. Exfoliated graphene is a large single crystal and hence it exhibits higher stiffness and modulus and hence the shift rates. In contrast, the CVD graphene exists as a continuous single-layer film with large number of smaller domains approximately 7 μm in diameter. The domain boundaries act as defects in the crystal structure[38,41] potentially meaning that each domain acts as an individual flake. Hence, shear lag theory would predict that there would be a lower strain at the edges of the domains, based upon a similar argument as that for the solvent exfoliated flakes (Supporting Information, S6). Furthermore, some domains could be small enough for edge effects to dominate so that full stress transfer does not occur within the flake, lowering the band shift rate. Another plausible reason for incomplete transfer of stress to the graphene CVD may be the poor interface being formed or wrinkling of the film taking place during the transfer process.

Bisset et al. recently showed that the G band upshift on tension in CVD graphene compared to a down shift in mechanically exfoliated graphene. They attributed this difference in behavior to the grain boundaries in the polycrystalline CVD graphene.[38] This anomalous behavior was not observed in the CVD graphene coatings herein, where a shift rate of ≈–14.72 cm^{-1}/% strain was observed when fitted with a single Lorentzian curve (see Supporting Information Figure S5). However, careful analysis of Bisset et al.'s experimental details show that their upshift is probably due to the fact that strain was not measured directly but rather inferred from the Raman peak shift, assuming the band shift per unit strain for a perfect crystal. The analysis of G band in our samples does however let the relative effects of doping and strain on the Raman spectra to be calculated as the G band is more sensitive to dopants than the 2D band (see Supporting Information, Figure S6). Based upon the G band peak shift, the hole doping level is estimated to be $<0.5 \times 10^{13}$ cm^{-2}. This level of doping would only give a 2D band shift of <1 cm^{-1}, which is significantly less than the 20 cm^{-1} shift observed from the applied strain (see Supporting Information).

2.4. Sensing Ability of the Coatings

The resolution and accuracy are the main two parameters that define the sensitivity of any strain sensor. The resolution is the smallest difference in relative strain that can be measured and is typically quoted in με. The accuracy is the repeatability in measure of an absolute strain from sample to sample and is typically quoted in percentage strain (1% ≡ 10^4 με). Commercially-available single-point strain sensors have very high resolutions up to 0.1 με, whereas large area photo-elasticity based strain sensors have relative resolutions ranging from 10–20 με and an absolute accuracy about 0.1%.[16]

The accuracy of measuring the strain in the graphene coatings could be determined from the cyclic deformational sequences. Absolute accuracy is given by the standard deviation of the difference of the 2D band position at one particular strain level divided by the ideal graphene shift rate of ≈ – 62 cm^{-1}/% strain as determined by using the Gruneisen parameter. The maximum achievable resolution (absolute resolution) of these graphene-based Raman strain sensors could be calculated from:

$$\text{Absolute resolution } (\mu\varepsilon) = \frac{\text{Absolute resolution of Raman spectrometer } (\text{cm}^{-1})}{\text{Maximum band shift obtained } (\text{cm}^{-1}/(\%\ \text{strain})} \times 10000 \quad (2)$$

Example calculations for both absolute accuracy and resolution are given in the Supporting Information, Section S5. The strain sensing ability of these graphene-based Raman strain sensors were calculated at two reference strain levels; 0.1% and 0.3% as shown in Figures 2a,d, 3a,d and at 0.3% in Figure 4a. It should be noted that, only the data where graphene in the composite coatings relaxed from its pre-strains were considered for the calculations (see Figures 2a,d, 3a,d, 4b). The calculated values of absolute accuracy and resolutions are given in **Table 1**.

Table 1. Calculated absolute accuracy and resolution of exfoliated and CVD graphene composite coatings.

Composites coatings	Deformational sequence	Absolute Accuracy [%]		Absolute resolution [με]
		@ 0.1 % strain	@ 0.3 % strain	
Mechanically exfoliated	Sequence I (Same max. strain)	≈ ± 0.04	≈ ± 0.02	≈15
	Sequence II (Increased max. strain)	≈ ± 0.03	≈ ± 0.02	≈18
CVD	Sequence I (Same max. strain)	≈ ± 0.01	≈ ± 0.01	≈27
	Sequence II (Increased max. strain)	≈ ± 0.01	≈ ± 0.01	≈27
	Sequence III	-	≈ ± 0.01	≈27

It can be observed from Table 1 that, the absolute accuracy and the resolution values changes between different deformation sequences. This is due to the deformation behavior of the graphene during the cyclic deformation. The variation in the absolute accuracy values of exfoliated graphene in sequences I and II could be attributed to the strain hardening behavior observed in the coatings. Whereas, as graphene relaxes from all the pre-strains and, the value of accuracy is constant at ≈ ± 0.02%, which is a better than the commercially-available large-area strain sensors. The maximum achievable resolutions of the exfoliated composites are in the range of ≈ 15–18 με which is comparable to the commercially-available large-area strain sensors. These high values correspond to a strong interface between the exfoliated graphene and the composite which leads to higher shift rates and hence high resolution. As discussed earlier, the CVD graphene has a lower resolution of ≈ 27 με, but still comparable to the exfoliated graphene. Nevertheless, the absolute accuracy values of CVD graphene after the relaxation of pre-strains stays around ≈ ± 0.01% for sequences I, II and III. It should be noted that, the maximum strain that these sensors could withstand is defined by the strain at the interface.

3. Conclusion

In this study, graphene coatings prepared from both exfoliated (top-down approach) and CVD methods (bottom-up approach) were demonstrated as Raman-based strain sensors by following the 2D band of graphene upon various cyclic deformation sequences. The CVD based coatings were found to have residual pre-compression stresses from their production method. However, these stresses relaxed over the first 2 to 3 deformation cycles, suggesting that sensors made from transferred graphene should be cycled by an external strain as a conditioning step during manufacture to ensure stable and accurate readings while in use. Moreover, hysteresis loop (interfacial damage) and its upshift were observed in exfoliated graphene coatings in the absence of residual pre-strains and exhibits strain hardening behavior with higher shift rates and effective modulus than CVD graphene. In general, the shift rates of exfoliated graphene are at least ≈35% higher than the CVD graphene, making the former more sensitive to strain, which may be due to exfoliated graphene being a large single crystal domain with high stiffness.

The absolute accuracy and resolution of these strain sensor coatings were calculated from the knowledge of 2D band position and absolute resolution of spectrometer. By comparing to the commercially available wide area strain sensors, CVD graphene films with a calculated absolute accuracy of ≈± 0.01% and absolute resolution of ≈ 27 με would be a promising candidate for a wide area Raman-based strain sensors.

4. Experimental Section

Graphene produced by two different methods; exfoliation and CVD technique was used to create the model coatings. The base specimen was prepared by spin coating 300 nm of SU-8 epoxy resin on a 5 mm thick PMMA beam as shown in Figure 1a.

Exfoliated Graphene Coatings: Graphene produced by mechanical cleavage of natural graphite was deposited on the base specimen (Figure 1a). This method produces various layers of graphene which could be identified using Raman spectroscopy.[31] A thin layer of around 100 nm of PMMA was spin coated on top of the specimen so that the graphene remain visible when sandwiched between two polymer layers.

CVD Graphene Preparation: CVD graphene was prepared using the hot wall CVD process.[42] The copper foils (Alfa Aesar product #13382) were cut into small squares and loaded into 1" fused silica furnace tube. The pressure in the tube was lowered by a rotary vane pump (Edwards RV12) in combination with a turbo pump (Leyboid Oerlikon Turbovac 50). Hydrogen was introduced in the furnace tube at 10 sccm for 30 min to displace any air in the tube. The hydrogen flow was then reduced to 1 sccm to achieve a pressure value of 5×10^{-3} mbar. Once the desired pressure was achieved, the temperature was increased to 1040 °C at a heating rate of 40 °C min^{-1} and the hydrogen flow was continued for 30 min to anneal the copper foil. The precursor methane was introduced at the rate of 2 sccm and the pressure maintained was about 0.01 mbar. After 30 min, the methane flow was terminated and the furnace was allowed to cool down in the room temperature. This process resulted in the formation of graphene on either side of the Cu foil, which was then carefully removed from the furnace tube.

CVD Graphene Coatings: The schematic representation of the transfer process is shown in Figure 1a. For the transfer process, a thin protective layer of ≈200 nm of PMMA was spin coated on one side of the Cu foil. Graphene on the other side of the foil was removed in an oxygen plasma for 5 min. The Cu was etched in a 0.1 M ammonium persulphate (etchant) solution, leaving PMMA/graphene film in the solution. The film was carefully transferred to deionised (DI) water to remove any residual etchant. This process was repeated several times to ensure the complete removal of etchant leaving behind film floating in the DI water. The base specimen was then used to carefully pick the floating film so that they lie in the middle of the beam. The sample was rested for 5 min before drying it oven at 70 °C for 10 min. The protective PMMA layer acts as the top layer of the coatings.

Deformation Sequences: The PMMA beams were deformed in a 4-point bending rig, and a strain gage (Vishay measurements) attached on the surface was used to monitor the surface strain. Three different cyclic deformation sequences were carried out in order to study the stress transfer and strain sensitivity of the graphene in the coatings:

I. Uniform maximum strain level – A total of four or five deformation cycles with a maximum strain level of 0.3% strain.
II. Increased maximum strain level – A total of five deformation cycles with 0.1%, 0.2%, 0.3%, 0.4%, and 0.5% strain as the maximum strain levels at each cycle.
III. Demonstration of longer term stability and spatial mapping: a total of 25 cycles with a maximum strain of 0.3%. 5 random points were studied at the maximum and minimum of each cycle. Detailed spatial maps were taken on initial, 6^{th} and 25^{th} cycles.

The maximum strain used in these deformation cycles were limited to 0.5% as the debonding of the flakes and matrix polymer cracking was observed at strains greater than 0.5% in similar model composites.[22,37] When the maximum strain was achieved in each cycle, the sample was unloaded step-wise to 0% strain.

Raman Spectroscopy: The Raman spectra was obtained from a low power (<1 mW) He-Ne laser (1.96 eV, 633 nm) in Renishaw 2000 spectrometer. The laser beam was always polarized parallel to the tensile axis and the spot size of laser was ≈2 μm with 50× objective lens. The shift of the 2D band with strain was used to follow the deformation. The deformation was carried out step-wise in intervals of either 0.02 or 0.05% strain. A total of three spectra at each strain level were taken and the average value was used for the calculations. The standard deviation was not shown in the deformation plots in order to follow the clear trend of deformations (see Supporting Information Figure S4). The 2D band spectra were fitted using single Lorentzian peak to determine the deformation behavior (see Supporting Information Figure S3). Splitting of the 2D band was not observed in this low strain range deformations as reported in the literature, however, broadening of 2D band was observed (Supporting Information Figure S3).[34]

Supporting Information

Supporting Information is available from the Wiley Online Library or from the author.

Acknowledgements

A.A. acknowledges the Dean of Engineering and Physical Science Faculty, University of Manchester for PhD Studentship and the EPSRC (Grants EP/I023879/1 and EP/G035954/1).

Received: August 15, 2013
Revised: November 11, 2013
Published online: February 6, 2014

[1] F. Schedin, A. Geim, S. Morozov, E. Hill, P. Blake, M. Katsnelson, K. Novoselov, *Nat. Mater.* **2007**, *6*, 652.
[2] T. Mueller, F. Xia, P. Avouris, *Nat. Photonics* **2010**, *4*, 297.
[3] F. Xia, T. Mueller, Y. Lin, A. Valdes-Garcia, P. Avouris, *Nat. Nanotechnol.* **2009**, *4*, 839.
[4] C. Chen, S. Rosenblatt, K. I. Bolotin, W. Kalb, P. Kim, I. Kymissis, H. L. Stormer, T. F. Heinz, J. Hone, *Nat. Nanotechnol.* **2009**, *4*, 861.
[5] M. Huang, T. A. Pascal, H. Kim, W. A. Goddard, J. R. Greer, *Nano Lett.* **2011**, *11*, 1241.
[6] Y. Wang, R. Yang, Z. Shi, L. Zhang, D. Shi, E. Wang, G. Zhang, *ACS Nano* **2011**, *5*, 3645.
[7] Y. Lee, S. Bae, H. Jang, S. Jang, S. E. Zhu, S. H. Sim, Y. I. Song, B. H. Hong, J. H. Ahn, *Nano Lett.* **2010**, *10*, 490.
[8] X. W. Fu, Z. M. Liao, J. X. Zhou, Y. B. Zhou, H. C. Wu, R. Zhang, G. Jing, J. Xu, X. Wu, W. Guo, *Appl. Phys. Lett.* **2011**, *99*, 213107.
[9] X. Li, R. Zhang, W. Yu, K. Wang, J. Wei, D. Wu, A. Cao, Z. Li, Y. Cheng, Q. Zheng, *Sci. Rep.* **2012**, *2*, 870.
[10] J. Zhao, C. He, R. Yang, Z. Shi, M. Cheng, W. Yang, G. Xie, D. Wang, D. Shi, G. Zhang, *Appl. Phys. Lett.* **2012**, *101*, 063112.
[11] S.-H. Bae, Y. Lee, B. K. Sharma, H.-J. Lee, J.-H. Kim, J.-H. Ahn, *Carbon* **2013**, *51*, 236.
[12] V. Eswaraiah, K. Balasubramaniam, S. Ramaprabhu, *J. Mater. Chem.* **2011**, *21*, 12626.
[13] Y.-J. Kim, J. Y. Cha, H. Ham, H. Huh, D.-S. So, I. Kang, *Curr. Appl. Phys.* **2011**, *11*, S350.
[14] M. Hempel, D. Nezich, J. Kong, M. Hofmann, *Nano Lett.* **2012**, *12*, 5714.
[15] S. Beeby, MEMS mechanical sensors, Artech House, Norwood, MA, USA **2004**.
[16] a) Vishay Precision Group, PhotoStress Analysis, http://www.vishaypg.com/micro-measurements/photo-stress-plus/ (accessed June, 2013); b) Stress Photonics, GFP 1000 – PSA, http://www.stressphotonics.com/PSA/PSA_Intro.html (accessed June, 2013).
[17] B. Lee, *Opt. Fiber Technol.* **2003**, *9*, 57.
[18] Q. Zhao, H. Daniel Wagner, *Compos., Part A* **2003**, *34*, 1219.
[19] P. Sureeyatanapas, R. J. Young, *Compos. Sci. Technol.* **2009**, *69*, 1547.
[20] Z. Li, P. Dharap, S. Nagarajaiah, E. V. Barrera, J. Kim, *Adv. Mater.* **2004**, *16*, 640.
[21] A. de la Vega, I. A. Kinloch, R. J. Young, W. Bauhofer, K. Schulte, *Compos. Sci. Technol.* **2011**, *71*, 160.
[22] L. Gong, I. A. Kinloch, R. J. Young, I. Riaz, R. Jalil, K. S. Novoselov, *Adv. Mater.* **2010**, *22*, 2694.
[23] R. J. Young, I. A. Kinloch, L. Gong, K. S. Novoselov, *Compos. Sci. Technol.* **2012**, *72*, 1459.
[24] G. Tsoukleri, J. Parthenios, K. Papagelis, R. Jalil, A. C. Ferrari, A. K. Geim, K. S. Novoselov, C. Galiotis, *Small* **2009**, *5*, 2397.
[25] O. Frank, G. Tsoukleri, I. Riaz, K. Papagelis, J. Parthenios, A. C. Ferrari, A. K. Geim, K. S. Novoselov, C. Galiotis, *Nat. Commun.* **2011**, *2*, 255.
[26] L. Gong, R. J. Young, I. A. Kinloch, I. Riaz, R. Jalil, K. S. Novoselov, *ACS Nano* **2012**, *6*, 2086.
[27] A. Reserbat-Plantey, L. Marty, O. Arcizet, N. Bendiab, V. Bouchiat, *Nat. Nanotechnol.* **2012**, *7*, 151.
[28] T. Kobayashi, M. Bando, N. Kimura, K. Shimizu, K. Kadono, N. Umezu, K. Miyahara, S. Hayazaki, S. Nagai, Y. Mizuguchi, *Appl. Phys. Lett.* **2013**, *102*, 023112.
[29] S. Bae, H. Kim, Y. Lee, X. Xu, J. S. Park, Y. Zheng, J. Balakrishnan, T. Lei, H. R. Kim, Y. I. Song, *Nat. Nanotechnol.* **2010**, *5*, 574.
[30] Bluestone Global Tech, Grat-Film, http://bluestonegt.com/products/grat-filmtm/ (accessed July, 2013).
[31] A. Ferrari, J. Meyer, V. Scardaci, C. Casiraghi, M. Lazzeri, F. Mauri, S. Piscanec, D. Jiang, K. Novoselov, S. Roth, *Phys. Rev. Lett.* **2006**, *97*, 187401.
[32] C. C. Kao, R. Young, *J. Mater. Sci.* **2010**, *45*, 1425.
[33] O. Frank, G. Tsoukleri, J. Parthenios, K. Papagelis, I. Riaz, R. Jalil, K. S. Novoselov, C. Galiotis, *ACS Nano* **2010**, *4*, 3131.
[34] T. Mohiuddin, A. Lombardo, R. Nair, A. Bonetti, G. Savini, R. Jalil, N. Bonini, D. Basko, C. Galiotis, N. Marzari, K. S. Novoselov, A. K. Geim, A. C. Ferrari, *Phys. Rev. B* **2009**, *79*, 205433.
[35] N. Ferralis, *J. Mater. Sci.* **2010**, *45*, 5135.

[36] J. Zabel, R. R. Nair, A. Ott, T. Georgiou, A. K. Geim, K. S. Novoselov, C. Casiraghi, *Nano Lett.* **2012**, *12*, 617.
[37] R. J. Young, L. Gong, I. A. Kinloch, I. Riaz, R. Jalil, K. S. Novoselov, *ACS Nano* **2011**, *5*, 3079.
[38] M. A. Bissett, W. Izumida, R. Saito, H. Ago, *ACS Nano* **2012**, *6*, 10229.
[39] N. Ferralis, R. Maboudian, C. Carraro, *Phys. Rev. Lett.* **2008**, *101*, 156801.
[40] J. A. Robinson, C. P. Puls, N. E. Staley, J. P. Stitt, M. A. Fanton, K. V. Emtsev, T. Seyller, Y. Liu, *Nano Lett.* **2009**, *9*, 964.
[41] P. Y. Huang, C. S. Ruiz-Vargas, A. M. van der Zande, W. S. Whitney, M. P. Levendorf, J. W. Kevek, S. Garg, J. S. Alden, C. J. Hustedt, Y. Zhu, *Nature* **2011**, *469*, 389.
[42] A. M. Lewis, B. Derby, I. A. Kinloch, *ACS Nano* **2013**, *7*, 3104.